Science of the Total Environment 924 (2024) 171687

Contents lists available at ScienceDirect

Science of the Total Environment

journal homepage: www.elsevier.com/locate/scitotenv

Co-occurrence of ozone and $PM_{2.5}$ pollution in urban/non-urban areas in eastern China from 2013 to 2020: Roles of meteorology and anthropogenic emissions

Huibin Dai [a], Hong Liao [a,*], Ye Wang [b], Jing Qian [a]

[a] Jiangsu Key Laboratory of Atmospheric Environment Monitoring and Pollution Control, Jiangsu Collaborative Innovation Center of Atmospheric Environment and Equipment Technology, School of Environmental Science and Engineering, Nanjing University of Information Science & Technology, Nanjing 210044, China
[b] Key Laboratory of Meteorological Disaster, Ministry of Education (KLME)/Joint International Research Laboratory of Climate and Environment Change (ILCEC)/ Collaborative Innovation Center on Forecast and Evaluation of Meteorological Disasters (CIC-FEMD), Nanjing University of Information Science and Technology, Nanjing 210044, China

HIGHLIGHTS

- In BTH and YRD, meteorology favored the increase in O_3-$PM_{2.5}$PD while emissions had an opposite impact in 2013–2020.
- The rise in T2m_max and T2m was key meteorological factors for O_3-$PM_{2.5}$PD in BTH and YRD.
- Cutting VOCs in BTH and YRD urban areas lowers both O_3-$PM_{2.5}$PD and oxidizing capacity.
- Synergistic NO_x and VOC cuts led to large O_3-$PM_{2.5}$PD drops in urban and non-urban areas.

GRAPHICAL ABSTRACT

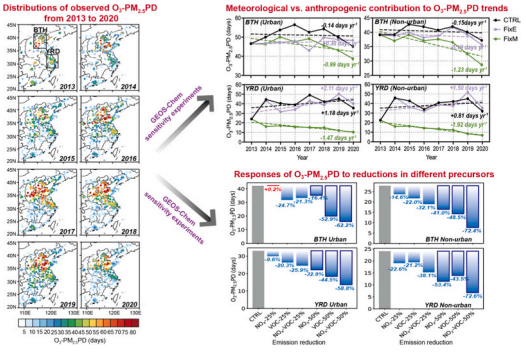

ARTICLE INFO

Editor: Jianmin Chen

Keywords:
Ozone and $PM_{2.5}$ pollution
Emission reductions
Meteorology

ABSTRACT

We applied a three-dimensional (3-D) global chemical transport model (GEOS-Chem) to evaluate the influences of meteorology and anthropogenic emissions on the co-occurrence of ozone (O_3) and fine particulate matter ($PM_{2.5}$) pollution day (O_3-$PM_{2.5}$PD) in urban and non-urban areas of the Beijing-Tianjin-Hebei (BTH) and Yangtze River Delta (YRD) regions during the warm season (April–October) from 2013 to 2020. The model captured the observed O_3-$PM_{2.5}$PD trends and spatial distributions well. From 2013 to 2020, with changes in both anthropogenic emissions and meteorology, the simulated values of O_3-$PM_{2.5}$PD in the urban (non-urban) areas of the BTH and YRD regions were 424.8 (330.1) and 309.3 (286.9) days, respectively, suggesting that pollution in non-urban areas also warrants attention. The trends in the simulated values of O_3-$PM_{2.5}$PD were −0.14 and −0.15 (+1.18 and +0.81) days yr^{-1} in the BTH (YRD) urban and non-urban areas, respectively. Sensitivity simulations revealed that changes in anthropogenic emissions decreased the occurrence of O_3-$PM_{2.5}$PD, with trends of −0.99 and −1.23 (−1.47 and −1.92) days yr^{-1} in the BTH (YRD) urban and non-urban areas, respectively. Conversely, meteorological conditions could exacerbate the frequency of O_3-$PM_{2.5}$PD, especially in the urban YRD areas, but less notably in the urban BTH areas, with trends of +2.11 and +0.30 days

* Corresponding author.
E-mail address: hongliao@nuist.edu.cn (H. Liao).

https://doi.org/10.1016/j.scitotenv.2024.171687
Received 27 November 2023; Received in revised form 25 February 2024; Accepted 10 March 2024
Available online 13 March 2024

yr^{-1}, respectively, owing to changes in meteorology only. The increases in T2m_max and T2m were the main meteorological factors affecting O_3-$PM_{2.5}$PD in most BTH and YRD areas. Furthermore, by conducting sensitivity experiments with different levels of pollutant precursor reductions in 2020, we found that volatile organic compound (VOC) reductions primarily benefited O_3-$PM_{2.5}$PD decreases in urban areas and that NO_x reductions more notably influenced those in non-urban areas, especially in the YRD region. Simultaneously, reducing VOC and NO_x emissions by 50 % resulted in considerable O_3-$PM_{2.5}$PD decreases (58.8–72.6 %) in the urban and non-urban areas of the BTH and YRD regions. The results of this study have important implications for the control of O_3-$PM_{2.5}$PD in the urban and non-urban areas of the BTH and YRD regions.

1. Introduction

In recent years, severe air pollution has occurred in China, which has attracted public and governmental attention. This phenomenon is mainly characterized by ozone (O_3) and fine particulate matter ($PM_{2.5}$) pollution. Since 2013, stringent clean air actions have been implemented to improve the air quality in China (State Council of the People's Republic of China, 2013, 2018). However, O_3 concentrations have rapidly increased in China, and the daily maximum 8-h average ozone (MDA8 O_3) concentration often exceeds Grade II (160 μg m^{-3}) of the Chinese Ambient Air Quality Standards (CAAQS) (Li et al., 2020). Additionally, $PM_{2.5}$ concentrations in China have remained persistently high, with 61.9 % of 168 key cities exceeding Grade I (35 μg m^{-3}) of the CAAQS in 2020 (Ministry of Ecology and Environment of the People's Republic of China, 2021). Notably, the co-occurrence of O_3 and $PM_{2.5}$ pollution day (O_3-$PM_{2.5}$PD; with a maximum daily 8 h average O_3 (MDA8 O_3) > 160 μg m^{-3} and $PM_{2.5}$ > 35 μg m^{-3}) has been frequently observed from April–October (Dai et al., 2021; Shao et al., 2022), especially in typical polluted areas in eastern China, including the Yangtze River Delta (YRD; 30–33°N, 119–122°E) and Beijing-Tianjin-Hebei (BTH; 34–41°N, 113–119°E) regions (Dai et al., 2023; Qin et al., 2021). Exposure to high surface O_3 and $PM_{2.5}$ concentrations is detrimental to human health (Yin et al., 2017; Y. Zhang et al., 2019; Q. Zhang et al., 2019), vegetation (Wang et al., 2018; Gong et al., 2021), and ecosystems (Yue et al., 2017). Therefore, understanding the variation in O_3-$PM_{2.5}$PD from 2013 to 2020 and delineating the respective roles of anthropogenic emissions and meteorological factors are important for developing effective pollution control strategies.

Few studies have focused on addressing the trends and characteristics of the co-occurrence of O_3 and $PM_{2.5}$ pollution in the YRD and BTH regions. Qin et al. (2021) utilized observations from the China National Environmental Monitoring Center (CNEMC) for 2015–2019 and reported that double-high pollution (DHP) events (defined as events characterized by MDA8 O_3 > 160 μg m^{-3} and $PM_{2.5}$ > 75 μg m^{-3}) mostly occurred in the northwestern YRD region, especially in spring (April) and autumn (October), and that the total number of DHP events in the YRD region decreased from 2015 to 2019. Ou et al. (2022) studied the observed co-pollution of O_3 and $PM_{2.5}$ (MDA8 O_3 > 160 μg m^{-3} and $PM_{2.5}$ > 35 μg m^{-3}) from May–September 2015–2019 across the BTH region and revealed that co-pollution has become the main type of air pollution during the high-temperature season since 2017, and most co-pollution is initiated by high O_3 concentrations during the day. Dai et al. (2023) applied a three-dimensional (3-D) global chemical transport model (GEOS-Chem) to investigate the chemical and physical characteristics of O_3 and $PM_{2.5}$ co-pollution days from 2013 to 2020 in the BTH region via composite analyses and found that co-polluted days often exhibited greater atmospheric oxidation, while secondary aerosols (nitrate, ammonium, and sulfate) experienced intense chemical production reactions at altitudes from 913 to 819 hPa, which were then transported downwards, resulting in relatively uniform vertical profiles on O_3 and $PM_{2.5}$ co-pollution days.

Several studies have investigated the favourable meteorological conditions for the co-occurrence of O_3 and $PM_{2.5}$ pollution. By using observation data from the CNEMC and China Meteorological Administration (CMA), Dai et al. (2021) reported that co-polluted days in the YRD region from 2013 to 2019 mainly occurred in April (29.6 % of the total co-polluted days occurred in April), May (23.0 %), June (19.5 %), and October (10.8 %), which were characterized by a higher relative humidity, an elevated surface air temperature, and a lower wind speed than days with O_3 pollution alone. Luo et al. (2022) used the T-mode principal component analysis (T-PCA) method and revealed that the observed shift in O_3 and $PM_{2.5}$ DHP events in the BTH region from summer to early spring of 2015–2019 was primarily influenced by the prevailing weather patterns, which resulted in higher temperatures and more intense radiation in early spring. Ma et al. (2023) analysed hourly O_3 and $PM_{2.5}$ data from the CNEMC and meteorological variables from the European Centre for Medium-Range Weather Forecasts (ECMWF) Reanalysis v5.0 dataset and reported that O_3 and $PM_{2.5}$ co-pollution in the BTH region from April–May from 2015 to 2019 occurred under hot, humid, and stagnant conditions, dominated by an anomalous anticyclonic circulation pattern over North China.

Apart from meteorological factors, O_3 and $PM_{2.5}$ co-pollution is significantly influenced by anthropogenic emissions. However, most research has focused only on examining the impact of anthropogenic emissions on O_3 or $PM_{2.5}$ pollution. With the utilization of the Community Multiscale Air Quality (CMAQ) modelling system model, Wang et al. (2019) demonstrated that emission reductions in 2014 and 2015 effectively reduced $PM_{2.5}$ concentrations in China by 23.9 and 43.5 μg m^{-3}, respectively, but these reductions were partially counteracted by unfavourable meteorological conditions. Dang et al. (2021) applied the GEOS-Chem model to examine the anthropogenic and meteorological contributions to the summertime O_3 trends in the BTH and YRD regions from 2012 to 2017 and reported that variations in both anthropogenic emissions and meteorological conditions contributed to the increase in MDA8 O_3 levels, with contributions of 39 % and 49 %, respectively, in the BTH region and 13 % and 84 %, respectively, in the YRD region. Ding et al. (2022) used the WRF-CMAQ model to evaluate strategies for synergistic reductions in the O_3 and $PM_{2.5}$ concentrations in the BTH region and discovered that a reduction in NO_x emissions (64 %–81 %) is crucial for meeting air quality standards and highlighted the necessity of simultaneous volatile organic compound (VOC) and NO_x emission control in winter while intensifying NO_x control in summer.

Previous studies have mostly focused on the characteristics and meteorological conditions of O_3 and $PM_{2.5}$ co-pollution and have mainly considered urban cities or entire areas of the BTH and YRD regions. However, due to the longer lifecycle of O_3, in addition to the occurrence of O_3 and $PM_{2.5}$ co-pollution in urban areas, pollution in non-urban areas should be investigated. Furthermore, almost no research has focused on investigating the impacts of meteorology and anthropogenic emissions on O_3 and $PM_{2.5}$ co-pollution in urban and non-urban areas, which is meaningful for systematically formulating regional joint prevention and control measures for such pollution events.

In this work, we utilized GEOS-Chem model to simulate the co-occurrence of O_3 and $PM_{2.5}$ pollution days in the urban and non-urban areas of the BTH and YRD regions from 2013 to 2020 and conducted multiple sensitivity experiments. The aims of this study were (1) to investigate the contributions of meteorological conditions and anthropogenic emissions to the trends in the co-occurrence of O_3 and $PM_{2.5}$ pollution days, (2) to identify the dominant meteorological variables on these co-pollution days, and (3) to assess effective emission reduction

strategies for controlling the co-occurrence of O_3 and $PM_{2.5}$ pollution days in both the urban and non-urban areas of the BTH and YRD regions.

2. Methods

2.1. Surface O_3 and $PM_{2.5}$ monitoring network

Hourly surface O_3 and $PM_{2.5}$ concentrations from 2013 to 2020 were obtained from the CNEMC (http://www.cnemc.cn; last access: 27 November 2023). To ensure the data quality, the MDA8 O_3 concentration was calculated only when the number of valid data points was at least 6 for each 8-hour interval, and the daily $PM_{2.5}$ concentration was calculated when the number of valid data points was at least 20 for each day. Additionally, the number of days with valid O_3 or $PM_{2.5}$ concentrations should be >15 each month. For model evaluation, the observations were averaged over the 0.5° latitude × 0.625° longitude model grid cells. Notably, the observed O_3 concentrations from the CNEMC are expressed in units of micrograms per cubic metre, under standard conditions of 273 K and 1013 hPa before 31 August 2018 and thereafter under reference conditions of 298 K and 1013 hPa (http://www.mee.gov.cn/, last access: 27 November 2023). To enable the analysis of long-term series and to ensure consistency between the observations and simulations, we converted the post-31 August 2018 O_3 concentrations to the standard conditions of 273 K and 1013 hPa.

2.2. Study areas

Following the above data quality control methods, we selected 79 valid observation sites in the BTH region (37–41°N, 114–118°E) and 154 valid sites in the YRD region (29–32.5°N, 116–123°E), as shown in Fig. 1. In addition to the selected observation sites, we considered the locations of the urban areas in the BTH and YRD regions. The definition of urban areas is based on the research of Sun et al. (2022) and can be obtained from http://www.doi.org/10.11922/. This dataset is the first globally developed Chinese urban dataset based on United Nations standards for built-up areas by using remote sensing technology. This dataset exhibits high accuracy and is widely applied in different studies. As shown in Fig. 1, most observation sites in the BTH and YRD regions occurred in urban areas, which could result in loss of information on rural regions. Therefore, it is important to exploit the model to study O_3 and $PM_{2.5}$ co-pollution in both the urban and non-urban areas of the BTH and YRD regions.

2.3. Meteorological data and multiple linear regression model

Meteorological parameters for 2013–2020 were retrieved from the Modern-Era Retrospective Analysis for Research and Applications (MERRA-2) dataset, which was generated by the NASA Global Modelling and Assimilation Office (GMAO), with a horizontal resolution of 0.5° latitude by 0.625° longitude. Following Li et al. (2019) and Dang et al. (2021), 15 meteorological parameters (Table S1) were considered original candidate meteorological predictors for the multiple linear regression (MLR) model.

The MLR model aims to establish a function between the response variable and several predictor variables and has been widely used to analyse the relationships between meteorological conditions and air pollutants (Shen et al., 2015; Yang et al., 2016; Chen et al., 2020; Dang et al., 2021; Qian et al., 2022). The MLR model can be expressed as follows:

$$y = \beta_0 + \sum_{k=1}^{N} \beta_k x_k + \varepsilon \quad (1)$$

where y is the MDA8 O_3 (or $PM_{2.5}$) concentration or the frequency of O_3 and $PM_{2.5}$ pollution days, x_k denotes a given meteorological predictor, as listed in Table S1, β_0 is the intercept term, β_k is the regression coefficient for the k-th meteorological predictor, and ε is the residual term. The meteorological variables statistically significant at the 95 % confidence level were retained as potential predictors for subsequent stepwise linear regression analysis. To minimize the influence of the correlations between the meteorological predictors, the variance inflation factor (VIF) was used to examine the multicollinearity problem (Altland, 1999; Che et al., 2019), and the VIF can be calculated as follows:

$$VIF = \frac{1}{1 - R_i^2} \quad (2)$$

where R_i^2 is the coefficient of determination obtained from the regression between the i-th meteorological predictor and the other meteorological predictors. We adopted a threshold value of 10 for the VIF to delineate the maximum acceptable level of collinearity. Consequently, any meteorological predictors exhibiting a VIF value exceeding this threshold were excluded from the analysis.

2.4. GEOS-Chem model

2.4.1. Model description

We simulated the O_3 and $PM_{2.5}$ concentrations using the nested-grid version of the GEOS-Chem model (version 11–01; http://acmg.seas.harvard.edu/geos/), which was driven by meteorological fields from the MERRA-2 dataset (Gelaro et al., 2017). The nested-grid domain was set over Asia (11°S–55°N, 60–150°E), with a horizontal resolution of 0.5° latitude by 0.625° longitude and 47 vertical layers up to an altitude of 0.01 hPa. The chemical boundary conditions for the gas and aerosol simulations of the nested grid were provided by coupled global GEOS-Chem simulations with a 2.5° latitude by 2.5° longitude horizontal resolution, and the model was spun up for 6 months before integration over the study period to ensure reliability.

The GEOS-Chem model includes a fully coupled HO_x–NO_x–VOC–O_3–aerosol chemical mechanism that includes approximately 300 chemical species involved in >400 kinetic and photolysis

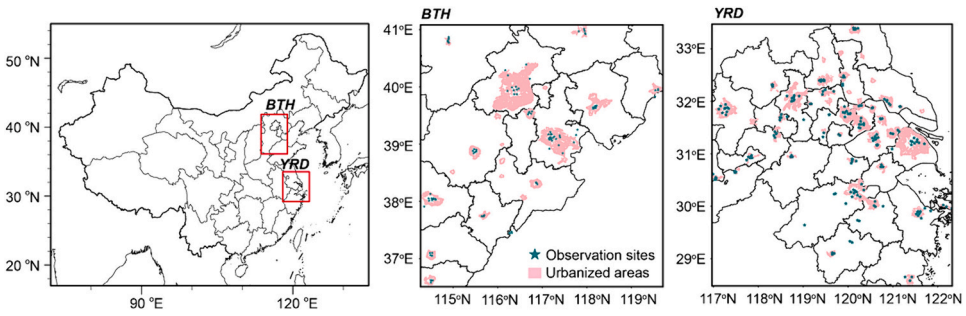

Fig. 1. BTH (37–41°N, 114–118°E) and YRD (29–32.5°N, 116–123°E) regions marked by red rectangles; the locations of the observation sites are indicated. The pentagrams indicate the observation sites, and the regions surrounded by pink indicate the urban areas of the BTH and YRD regions.

reactions (Bey et al., 2001; Pye et al., 2009; Mao et al., 2013). The $PM_{2.5}$ components simulated in the GEOS-Chem model include sulfate (Park, 2004), nitrate (Pye et al., 2009), ammonium, black carbon (BC), primary organic carbon (OC) (Park, 2003), mineral dust (Fairlie et al., 2007), and sea salt (Alexander et al., 2005). Considering that mineral dust and sea salt aerosols are not the major components in China and that their concentrations are generally low according to previous measurements (Xuan et al., 2000; Ye et al., 2003; Duan et al., 2006; Zhao et al., 2013), we calculated the $PM_{2.5}$ concentration in this study as the sum of the sulfate, nitrate, ammonium, BC, and OC masses.

2.4.2. Emissions

Global anthropogenic emissions were sourced from the Community Emissions Data System (CEDS) developed by Hoesly et al. (2018). Within the Asian domain, specifically for China, anthropogenic emissions were acquired from the Multiresolution Emission Inventory for China (MEIC), which includes the anthropogenic emissions of OC, BC, carbon monoxide (CO), sulfur dioxide (SO_2), NO_x, ammonia (NH_3), and VOCs from the agriculture, industry, power, residential, and transportation sectors for 2013–2020 (Li et al., 2017; Zheng et al., 2018; Zheng et al., 2021). Biogenic emissions in the GEOS-Chem model were calculated online with the Model of Emissions of Gases and Aerosols from Nature (MEGAN v2.1), following Guenther et al. (2012).

Fig. 2 shows the variations in the anthropogenic emissions of O_3 precursors, aerosols, and aerosol precursors in the BTH and YRD regions from 2013 to 2020 during the warm season (April–October) obtained from the MEIC. During this period, a general downward trend in most anthropogenic emissions was observed in both the BTH and YRD regions, with the greatest reduction noted in SO_2 emissions. This significant decrease could be attributed to the stringent emission control measures implemented to improve the air quality in China since 2013 (State Council of the People's Republic of China, 2013, 2018). However, the NH_3 emissions did not exhibit a clear trend, reflecting the relative stability of agricultural sources. Comparatively, by 2020, the emissions of BC, NH_3, NO_x, OC, SO_2, and nonmethane VOC (NMVOC) in the BTH (YRD) region decreased by 48.2 % (42.4 %), 8.2 % (14.7 %), 31.9 % (30.5 %), 47.9 % (42.6 %), 79.6 % (80.3 %), and 4.9 % (1.5 %), respectively, relative to 2013 levels. The variations in emissions obtained in this study are consistent with the results of Zheng et al. (2021).

2.4.3. Numerical experiments

To investigate the relative effects of changes in anthropogenic emissions and meteorological parameters on O_3-$PM_{2.5}$PD during the warm season from 2013 to 2020, as well as to assess the impact of the reduction in the emissions of each precursor on O_3-$PM_{2.5}$PD, we conducted multiple sensitivity simulation experiments using the GEOS-Chem model. The results are presented in Table 1. The standard simulation (CTRL) included variations in both anthropogenic emissions and meteorological fields over the 2013–2020 period. The FixE (FixM) simulation was the same as the CTRL experiment but with the anthropogenic emissions (meteorological fields) fixed at 2013 levels. The FixE and FixM simulations were designed to investigate the impacts of changes in the meteorological parameters and anthropogenic emissions on O_3-$PM_{2.5}$PD from 2013 to 2020, respectively.

Moreover, to determine the specific impacts of the main pollutant precursors on O_3-$PM_{2.5}$PD, we conducted ten additional sensitivity simulations using the GEOS-Chem model. It was estimated that the anthropogenic NO_x, SO_2, VOC and NH_3 emissions decreased by 38 %, 51 %, 11 % and 17 %, respectively, in China, owing to China's Air Pollution Control Plan and the Three-Year Action Plan from 2013 to 2019 (Jiang et al., 2022). Therefore, our experiments assumed reasonable reductions of 25 % and 50 % in precursors (i.e., NH_3–25 %, NO_x-25 %, SO_2–25 %, VOC-25 %, NH_3–50 %, NO_x-50 %, SO_2–50 %, VOC-50 %, NOx-VOC-25 %, and NOx-VOC-50 %) to investigate the responses of O_3-$PM_{2.5}$PD to reductions in different precursors. The contribution of the reduction in emissions of each precursor to O_3-$PM_{2.5}$PD mitigation was obtained by comparing the results of each sensitivity simulation with those of the

Table 1
Configurations of the GEOS-Chem simulations in this study.

Simulation	Meteorologi-cal fields	Anthropogenic emissions
CTRL	2013–2020	2013–2020
FixE	2013–2020	2013
FixM	2013	2013–2020
NH_3–25 (50) %	2020	25 (50) % reduction in NH_3 in 2020
NO_x-25 (50) %	2020	25 (50) % reduction in NO_x in 2020
SO_2–25 (50) %	2020	25 (50) % reduction in SO_2 in 2020
VOC-25 (50) %	2020	25 (50) % reduction in VOC in 2020
NO_x-VOC-25 (50) %	2020	25 (50) % reduction in NO_x and VOC in 2020

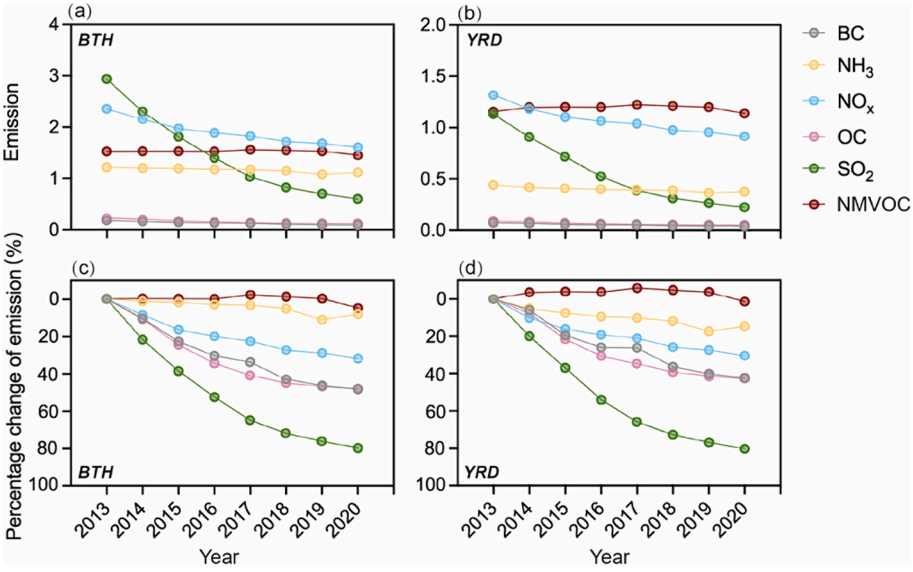

Fig. 2. Changes in the anthropogenic emissions of BC, NH_3, NO_x, OC, SO_2 and NMVOC (unit: Tg) during the warm season (April–October) in (a) the BTH and (b) YRD regions from 2013 to 2020; percentage changes in these emissions compared to the baseline values in 2013 (unit: %) in (c) the BTH and (d) YRD regions.

CTRL simulation. The year 2020 was selected for these emission reduction simulations as it represents the most recent year with emission data available from the MEIC, providing a relevant and contemporary basis for evaluating and developing future emission abatement policies.

3. Results and discussion

3.1. Observed O_3 and $PM_{2.5}$ pollution days

Fig. 3 shows the spatial and temporal distributions of the observed O_3 and $PM_{2.5}$ pollution days over the April–October period from 2013 to 2020, with the $PM_{2.5}$ concentrations exceeding the CAAQS Grade II (75 μg m^{-3}) and Grade I (35 μg m^{-3}) standards, respectively. The numbers of both O_3-$PM_{2.5}$PD-75 and O_3-$PM_{2.5}$PD were larger in the BTH region than in the YRD region, which could be attributed to the higher levels of anthropogenic emissions in the BTH region (Dang et al., 2021). As shown in Fig. 3a, between 2013 and 2020, there was a marked decrease in the number of O_3-$PM_{2.5}$PD-75 in both the BTH and YRD regions, with the average number of O_3-$PM_{2.5}$PD-75 in the BTH region (YRD) decreasing from 41.2 (20.3) days in 2013 to 8.5 (4.7) days in 2020. The observed significant decrease in O_3-$PM_{2.5}$PD-75 primarily resulted from reduced $PM_{2.5}$ concentrations, attributable to the stringent emission controls on primary particulate matter and SO_2 implemented since 2013 (Zheng et al., 2018; Y. Zhang et al., 2019; Q. Zhang et al., 2019), coupled with the generally lower $PM_{2.5}$ concentrations during the warm season.

Notably, as shown in Fig. 3b, the variation in the number of O_3-$PM_{2.5}$PD differed significantly from that of O_3-$PM_{2.5}$PD-75. In the BTH and YRD regions, the number of O_3-$PM_{2.5}$PD did not decrease from 2013 to 2020. Instead, there was a period of more intense pollution from 2016 to 2018. Therefore, investigating the primary factors influencing the fluctuations in O_3-$PM_{2.5}$PD, along with assessing the effect of emission reductions of various precursors on O_3-$PM_{2.5}$PD reduction, has significant implications for the prevention and control of complex air pollution conditions in China.

3.2. Simulated pollution days and model evaluation

3.2.1. Simulated MDA8 O_3 and $PM_{2.5}$ concentrations

Fig. 4 shows a comparison of the time series of the simulated and observed daily mean surface-layer MDA8 O_3 and $PM_{2.5}$ concentrations in the BTH and YRD regions from 2013 to 2020. The model generally captured the daily variations (peaks and troughs) in the observed MDA8 O_3 and $PM_{2.5}$ concentrations well, with correlation coefficients (R values) of 0.8 and 0.72 for MDA8 O_3 and $PM_{2.5}$, respectively, in the BTH region and 0.7 and 0.71, respectively, in the YRD region. The simulated daily MDA8 O_3 ($PM_{2.5}$) concentrations during the eight warm seasons from 2013 to 2020 exhibited a normalized mean bias of +7.9 % (+10.6 %) in the BTH region and +17.3 % (−3.1 %) in the YRD region. The model performance obtained in this study closely agreed with the findings of previous work also utilizing the GEOS-Chem model (Dang and Liao, 2019; Gong and Liao, 2019; Dai et al., 2023). Overall, the model exhibited a favourable ability to reproduce the observed variations in the MDA8 O_3 and $PM_{2.5}$ concentrations.

3.2.2. Simulated O_3 and $PM_{2.5}$ pollution days

Fig. 5 shows the ability of the GEOS-Chem model for capturing the observed O_3 and $PM_{2.5}$ pollution days. The frequency of the observed O_3-$PM_{2.5}$PD was highest in the BTH region, as shown in Fig. 5a, and the spatial distribution of these pollution days was captured relatively well by the GEOS-Chem model. The total numbers of the observed and simulated O_3-$PM_{2.5}$PD summed over April–October 2013–2020 were 369 and 377 days, respectively, averaged across the BTH region and 223 and 297 days, respectively, averaged across the YRD region. Notably, the numbers of the simulated O_3-$PM_{2.5}$PD in the urban (non-urban) areas of the BTH and YRD regions were 424.8 (330.1) and 309.3 (286.9) days, respectively, suggesting that pollution in non-urban areas should also be considered.

Fig. 5b shows a comparison of the temporal evolution patterns of both the observed and simulated frequencies of O_3-$PM_{2.5}$PD in the BTH and YRD regions from 2013 to 2020. The GEOS-Chem model generally reproduced the observed annual variations in O_3-$PM_{2.5}$PD in the BTH and YRD regions, with a slight underestimation of the number of O_3-$PM_{2.5}$PD, especially in the BTH region. This underestimation mainly resulted from the deficiency of the model in capturing the peak O_3 and $PM_{2.5}$ concentrations, which has also been reported in previous studies using the GEOS-Chem model or the Weather Research and Forecasting with Chemistry (WFR-chem) model (Zhang and Wang, 2016; Ni et al., 2018; Gong and Liao, 2019; Dang and Liao, 2019). In general, the GEOS-Chem model could capture the spatial distribution and annual changes in the observed O_3-$PM_{2.5}$PD in the BTH and YRD regions from April to October 2013–2020.

3.3. Meteorological vs. anthropogenic contributions to the O_3-$PM_{2.5}$PD trends from 2013 to 2020

The impacts of meteorological factor and anthropogenic emission changes on the O_3-$PM_{2.5}$PD trends in the BTH and YRD regions from 2013 to 2020 are shown in Fig. 6. In the CTRL simulation experiment (Fig. 6a), the spatial distribution of O_3-$PM_{2.5}$PD influenced by both emissions and meteorological changes agreed with that of the observations, showing particular severity in eastern China, especially in the BTH region, and was accompanied by obvious interannual variations from 2013 to 2020. Moreover, the variations in the spatial and temporal distributions of O_3-$PM_{2.5}$PD determined in the FixE simulation experiment (Fig. 6b) were similar to those determined in the CTRL simulation experiment, indicating that changes in meteorological fields primarily drove the interannual variations in O_3-$PM_{2.5}$PD. Conversely, the FixM simulation experiment (Fig. 6c) demonstrated a steady decline in O_3-

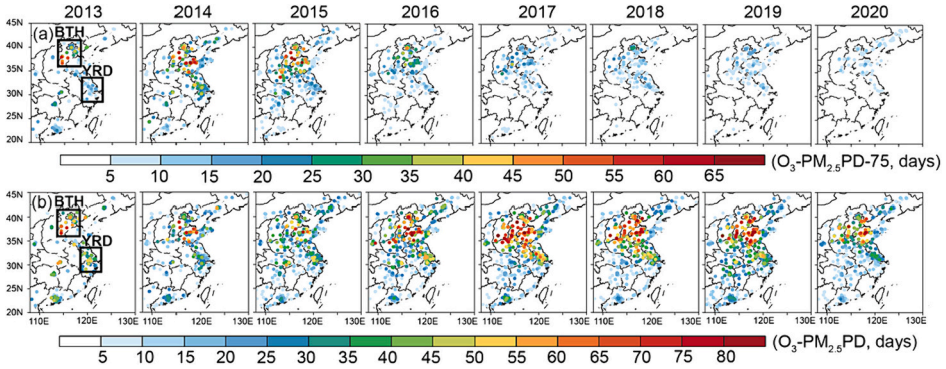

Fig. 3. Spatial distributions of the observed numbers of (a) O_3-$PM_{2.5}$PD-75 (MDA8 O_3 > 160 μg m^{-3} and $PM_{2.5}$ > 75 μg m^{-3}) and (b) O_3-$PM_{2.5}$PD (MDA8 O_3 > 160 μg m^{-3} and $PM_{2.5}$ > 35 μg m^{-3}) in eastern China from April–October 2013 to 2020. The solid black rectangles indicate the BTH and YRD regions.

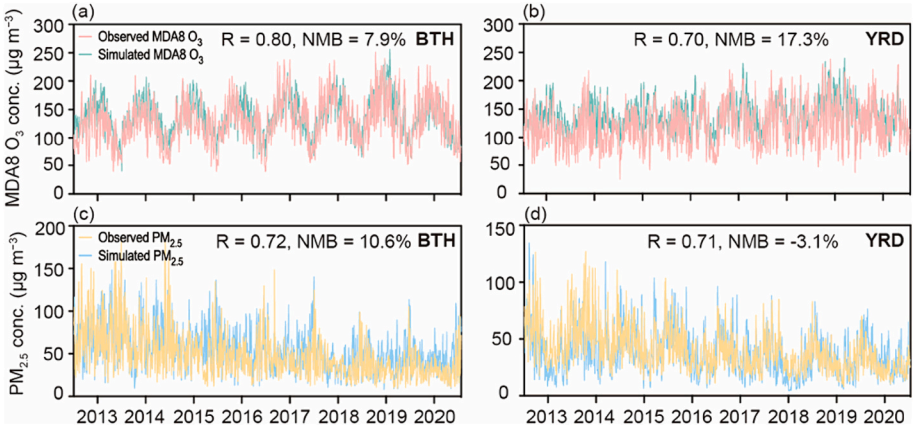

Fig. 4. Daily surface-layer simulated and observed MDA8 O_3 (a-b) and $PM_{2.5}$ (c-d) concentrations, averaged over the BTH and YRD regions from April to October 2013–2020. The correlation coefficient (R) and normalized mean bias (NMB) values are also shown, with NMB = $(\sum_{i=1}^{N}(M_i - O_i)/\sum_{i=1}^{N}(O_i)) \times 100$ %, where O_i and M_i are the observed and simulated concentrations, respectively, i denotes the i^{th} day, and N is the total number of days.

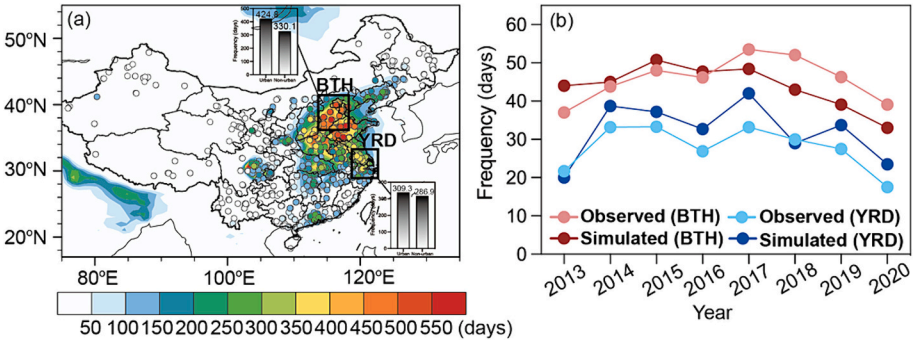

Fig. 5. (a) Spatial distributions of the simulated (CTRL, shaded) and observed (CNEMC, dots) numbers of O_3-$PM_{2.5}$PD summed over April–October 2013–2020. The solid black rectangles indicate the BTH and YRD regions, and the black shaded bars denote the number of O_3-$PM_{2.5}$PD (days) in the urban and non-urban areas. (b) Temporal evolution of the frequency of O_3-$PM_{2.5}$PD in the BTH and YRD regions from 2013 to 2020 derived from the observations and model simulations.

$PM_{2.5}$PD without interannual fluctuations, highlighting the significant impact of anthropogenic emission changes on decreasing the number of O_3-$PM_{2.5}$PD from 2013 to 2020.

Fig. 6d–g show the O_3-$PM_{2.5}$PD trends in the urban and non-urban areas of the BTH and YRD regions from 2013 to 2020 derived from the CTRL, FixE, and FixM simulations. In the urban and non-urban areas of the BTH region, the number of O_3-$PM_{2.5}$PD showed a slight downward trend in the CTRL simulation experiment, decreasing by −0.14 and −0.15 days yr^{-1}, respectively. In the FixM simulation experiment (i.e., with changes in emissions only from 2013 to 2020), the number of O_3-$PM_{2.5}$PD exhibited decreasing trends of −0.99 and −1.23 days yr^{-1}, respectively. In the FixE simulation experiment (i.e., with changes in meteorological fields only from 2013 to 2020), the number of O_3-$PM_{2.5}$PD increased by +0.30 and −0.19 days yr^{-1}, respectively. In contrast, in the urban (non-urban) areas of the YRD region, the frequency of O_3-$PM_{2.5}$PD determined in the CTRL, FixM, and FixE simulations exhibited trends of +1.18 (+0.81), −1.74 (−1.92), and +2.11 (+1.50) days yr^{-1}, respectively.

Overall, from 2013 to 2020, changes in anthropogenic emissions resulted in a significant decrease in the number of O_3-$PM_{2.5}$PD in the BTH and YRD regions, with a more pronounced reduction in the non-urban areas than in the urban areas, which is likely due to the different sensitivities of O_3 to NO_x and VOCs (with urban areas more sensitive to VOCs and rural areas more sensitive to NO_x). Conversely, meteorological conditions exerted different impacts on the trends in O_3-$PM_{2.5}$PD in the BTH and YRD regions. In the BTH region, the impact was minimal, while in the YRD region, meteorological conditions contributed significantly to the increase in O_3-$PM_{2.5}$PD, indicating that the meteorological conditions in the YRD region from 2013 to 2020 were relatively favourable for the occurrence of O_3-$PM_{2.5}$PD.

Fig. 7 shows the trends in the MDA8 O_3 and $PM_{2.5}$ concentrations obtained in the CTRL, FixM, and FixE simulations. From 2013 to 2020, the MDA8 O_3 concentrations in both the urban and non-urban areas of the BTH and YRD regions showed significant increasing trends, with increases of +1.10 ppb yr^{-1} in the BTH region and +0.93 ppb yr^{-1} in the YRD region. These increases were primarily driven by anthropogenic emission changes and were more notable in the urban areas than in the non-urban areas. Moreover, the $PM_{2.5}$ concentrations across the BTH and YRD regions dramatically decreased, with trends of −5.25 μg m^{-3} yr^{-1} in the urban BTH areas and −1.96 μg m^{-3} yr^{-1} in the urban YRD areas, respectively, which was attributable to the combined influence of anthropogenic emissions and meteorological conditions. The trend in the non-urban areas mirrored that in the urban areas but exhibited a lower value. Therefore, the increase in the MDA8 O_3 concentration was the primary factor driving the increase in O_3-$PM_{2.5}$PD, while the decrease in the $PM_{2.5}$ concentration exerted the opposite effect. As shown in Fig. S1, from 2013 to 2020, the increasing trend in O_3-$PM_{2.5}$PD in the urban YRD areas (+1.18 days yr^{-1}) was largely driven by the change in the MDA8 O_3 concentration, with a strong positive correlation of +0.86. In contrast, the trend in O_3-$PM_{2.5}$PD in the urban BTH areas (+0.30 days yr^{-1}) was partially influenced by the increase in the MDA8 O_3 concentration (correlation of +0.72) and significantly affected by the notable decrease in the $PM_{2.5}$ concentration (correlation of −0.80), resulting in a slight upward trend.

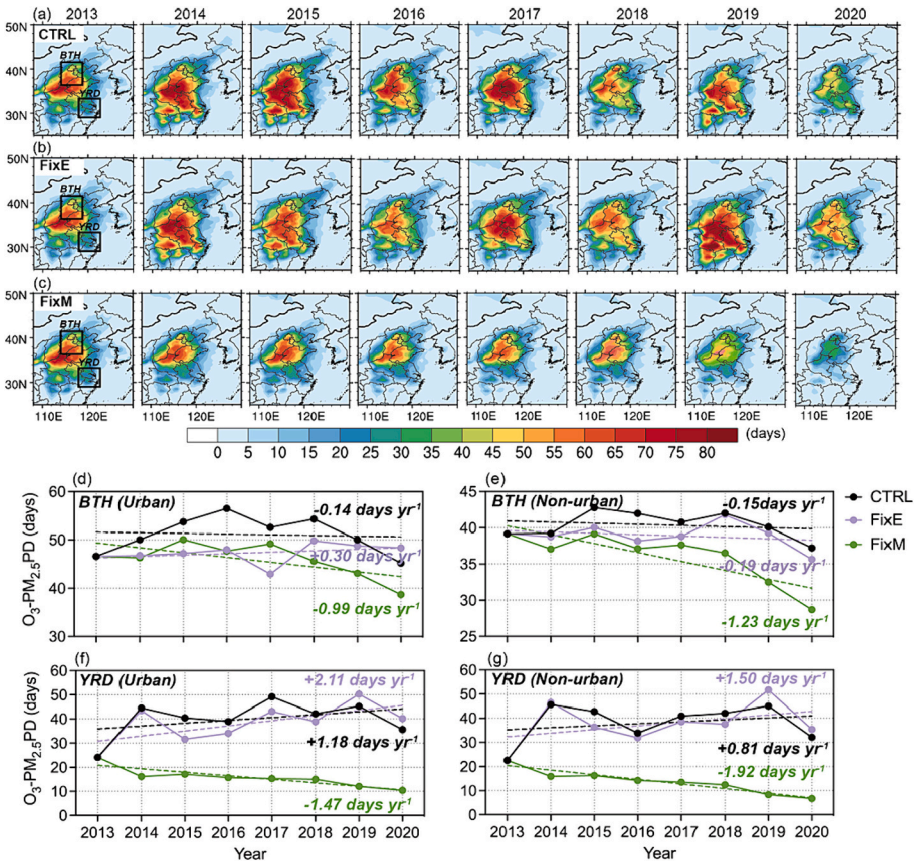

Fig. 6. Spatial distributions of the frequency of O_3-$PM_{2.5}$PD (days) from the (a) CTRL, (b) FixE, and (c) FixM simulations over 2013–2020; the solid black rectangles indicate the BTH and YRD regions. O_3-$PM_{2.5}$PD frequency trends (days yr^{-1}) in (d) the urban BTH, (e) non-urban BTH, (f) urban YRD, and (g) non-urban YRD areas from the CTRL, FixM, and FixE simulations.

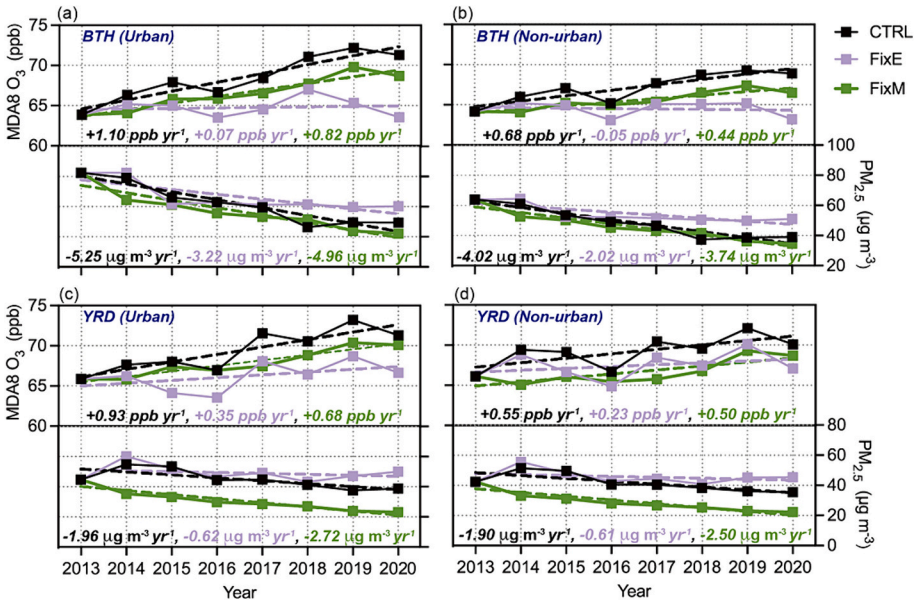

Fig. 7. Trends in the MDA8 O_3 (ppb yr^{-1}) and $PM_{2.5}$ (μg m^{-3} yr^{-1}) concentrations from 2013 to 2020 in the (a) urban BTH, (b) non-urban BTH, (c) urban YRD, and (d) non-urban YRD areas from the CTRL, FixM, and FixE simulation experiments.

3.4. Impacts of the key meteorological parameters on O_3-$PM_{2.5}$PD

Thus far, we have examined the influences of meteorological fields and anthropogenic emissions on the O_3-$PM_{2.5}$PD variations from 2013 to 2020 by employing modelling simulations, and the results showed that meteorological conditions greatly affected the annual fluctuations and overall increasing trend in O_3-$PM_{2.5}$PD. Therefore, we further investigated the key meteorological parameters influencing the observed O_3-

$PM_{2.5}$PD variations using the MLR approach, and the meteorological predictors are listed in Table S1. Here, only the top three meteorological predictors selected by the MLR model were used to avoid data overfitting (Li et al., 2019). To isolate the effects of the various meteorological factors, the MDA8 O_3 and $PM_{2.5}$ concentrations utilized in the MLR model were derived from the FixE simulation from 2013 to 2020.

Fig. 8 shows the spatial distribution, regression coefficient, and trends in the top meteorological factors identified by the MLR model as most significantly influencing the MDA8 O_3 and $PM_{2.5}$ concentrations and O_3-$PM_{2.5}$PD in the BTH region from 2013 to 2020. In most urban areas of the BTH region, T2m and T2m_max primarily affected the MDA8 O_3 concentrations, while RH_1000 and planetary boundary layer height (PBLH) were important for the $PM_{2.5}$ concentrations, and T2m was crucial for O_3-$PM_{2.5}$PD. The patterns of the top meteorological factors influencing the MDA8 O_3 concentration and O_3-$PM_{2.5}$PD were relatively similar. The increase in T2m_max and T2m (Fig. 8g and i) from 2013 to 2020 was the main reason for the increase in the meteorologically driven MDA8 O_3 concentration and O_3-$PM_{2.5}$PD, whereas the decrease in RH1000 and increase in PBLH (Fig. 8h) were the two major contributors to the decrease in the meteorologically driven $PM_{2.5}$ concentration. Additionally, the second and third key meteorological factors identified by the MLR model are shown in Figs. S2 and S4, respectively. These factors varied across the different areas and did not contribute to an increase in O_3-$PM_{2.5}$PD, which partly explained why the meteorologically driven trends in O_3-$PM_{2.5}$PD were relatively low, with values of +0.3 and −0.19 days yr^{-1} in the urban and non-urban areas (Fig. 6d and e), respectively.

In the YRD region, as shown in Fig. 9, the main meteorological factors in most urban areas during the warm months from 2013 to 2020 were T2m_max for the MDA8 O_3 concentration, U500 and U10 for the $PM_{2.5}$ concentration, and T2m_max and V10 for the number of O_3-$PM_{2.5}$PD. The changes in the top key meteorological factors between 2013 and 2020 significantly contributed to the increases in the MDA8 O_3 and $PM_{2.5}$ concentrations and O_3-$PM_{2.5}$PD over the YRD region. The second and third key meteorological factors influencing O_3-$PM_{2.5}$PD in the YRD region identified by the MLR model (shown in Figs. S3 and S5), mainly U500, SWGDN, T2m, and T2m_max, varied across the YRD region and largely contributed to the increasing trend in the meteorologically driven O_3-$PM_{2.5}$PD. The variations in the top three key meteorological factors in the YRD region were instrumental in increasing the number of O_3-$PM_{2.5}$PD by 2.11 days yr^{-1} in the urban areas and 1.5 days yr^{-1} in the non-urban areas, as shown in Fig. 6f and g, respectively.

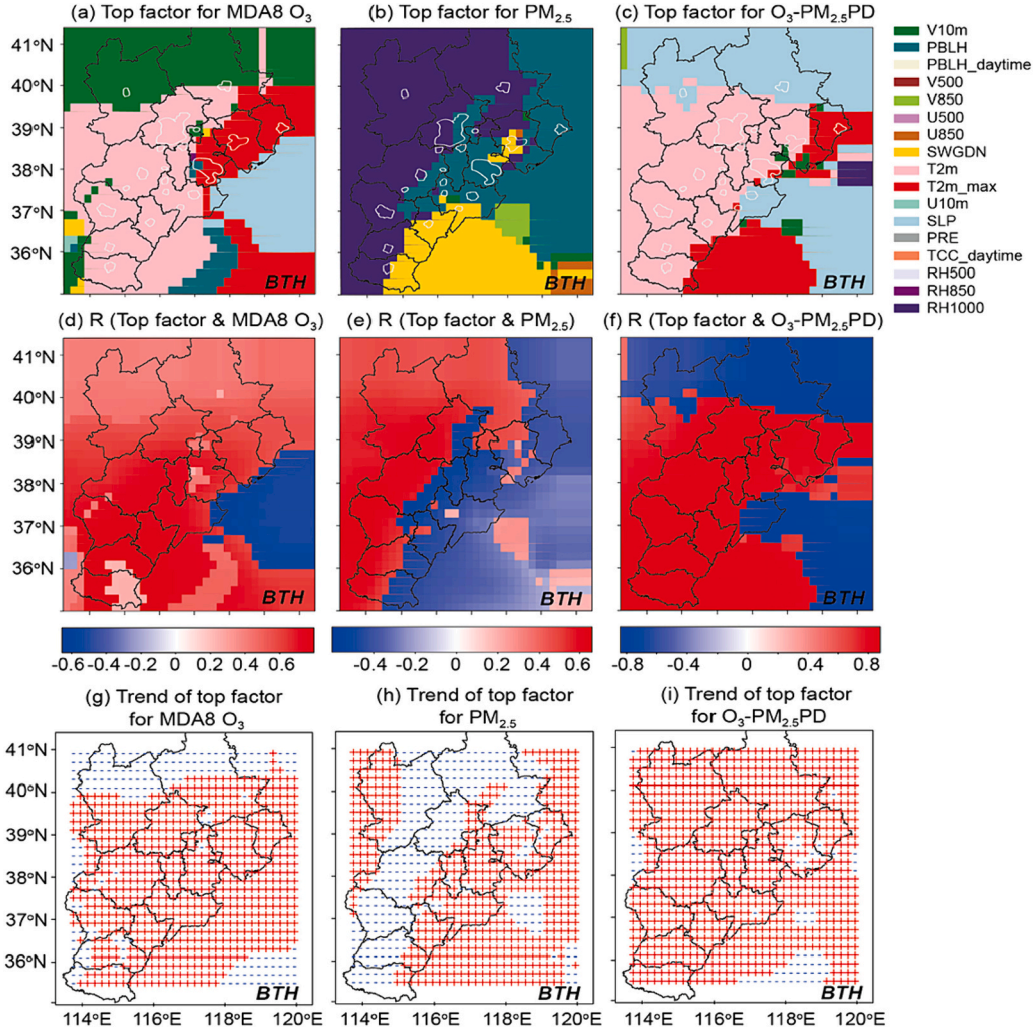

Fig. 8. (a)–(c) Spatial distribution of the top meteorological factors influencing the MDA8 O_3 and $PM_{2.5}$ concentrations and O_3-$PM_{2.5}$PD in the BTH region from 2013 to 2020, with the urban areas outlined in white. (d)–(f) Regression coefficients of the top meteorological factors with the MDA8 O_3 and $PM_{2.5}$ concentrations and O_3-$PM_{2.5}$PD in the MLR model. (g)–(i) Trends in the top meteorological factors, where the red "+" and blue "-" symbols indicate increasing and decreasing trends, respectively, from 2013 to 2020.

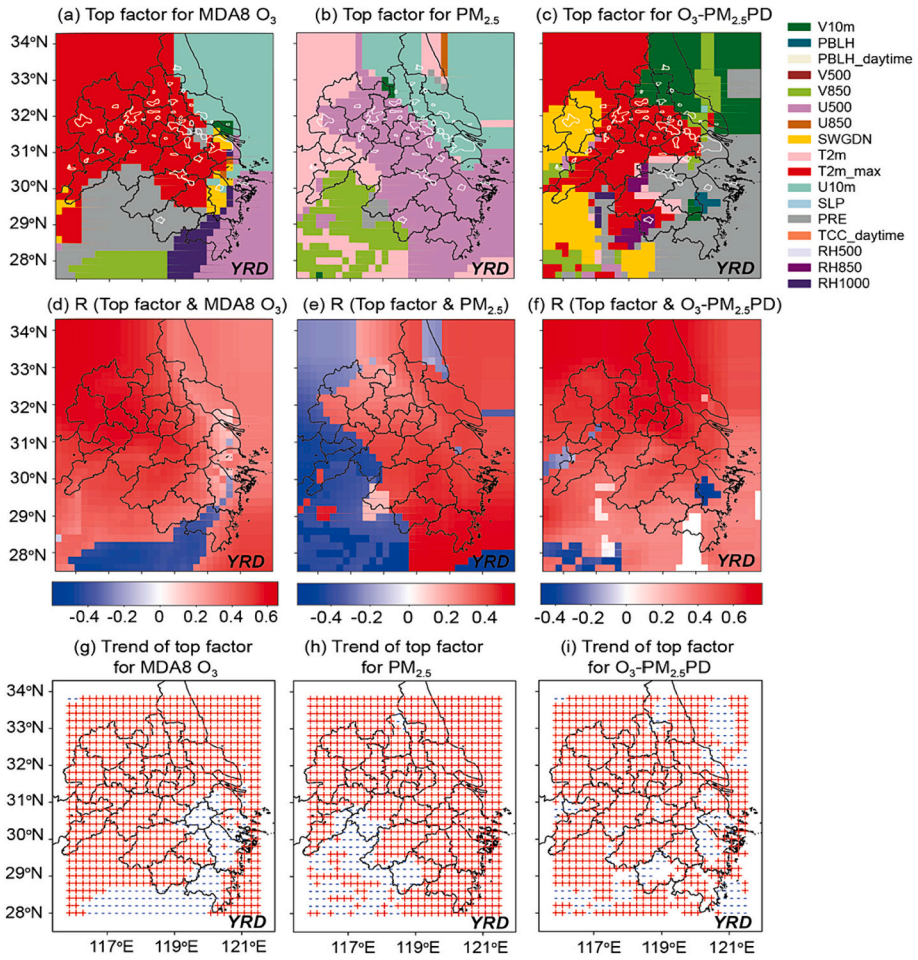

Fig. 9. Same as Fig. 8 but for the YRD region.

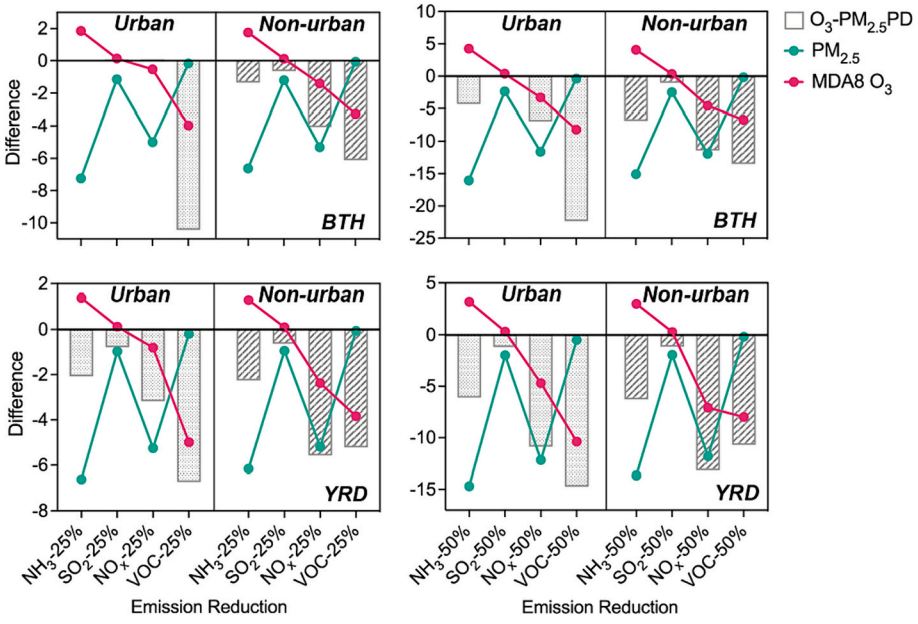

Fig. 10. Differences in O_3-$PM_{2.5}$PD (grey bordered column, days), MDA8 O_3 concentrations during O_3-$PM_{2.5}$PD (green dotted line, ppb), and $PM_{2.5}$ concentrations during O_3-$PM_{2.5}$PD (pink dotted line, μg m^{-3}) between the experiments with reductions of 25 % and 50 % in NH_3, SO_2, NO_x, and VOC emissions and the CTRL simulation experiment from April–October 2020 averaged over the urban and non-urban areas in the BTH and YRD regions.

3.5. Impact of anthropogenic emissions on O_3-$PM_{2.5}$PD

Apart from meteorological influences, anthropogenic emissions play an important role in determining the occurrence of O_3-$PM_{2.5}$PD. Therefore, we investigated the effect of reducing the emissions of various pollutant precursors on O_3-$PM_{2.5}$PD, and the detailed design of the experiments is described in Sec. 2.4.3.

Fig. 10 shows the differences in the number of O_3-$PM_{2.5}$PD and the MDA8 O_3 and $PM_{2.5}$ concentrations during O_3-$PM_{2.5}$PD between the eight emission reduction experiments and the CTRL simulation experiment, averaged over the urban and non-urban areas of the BTH and YRD regions. The distributions in the BTH and YRD regions are shown in Figs. S6–S8. In the BTH region, the reduction in VOC emissions significantly contributed to the decrease in O_3-$PM_{2.5}$PD, with a greater effect in the urban areas, largely through reducing MDA8 O_3 levels. In the YRD region, VOC abatement primarily influenced the reduction in O_3-$PM_{2.5}$PD in the urban areas, while NO_x abatement was more effective in the non-urban areas. The different impacts of emission reductions on O_3-$PM_{2.5}$PD in the different areas could be attributed to the nonlinear responses of MDA8 O_3 to NO_x and VOCs, as shown in Figs. S6 and S7, respectively, where the spatial patterns of the effects of emission reductions on MDA8 O_3 agreed with those of the effects on O_3-$PM_{2.5}$PD. In contrast, $PM_{2.5}$ demonstrated a uniform response to emission reductions in both the urban and non-urban areas in the BTH and YRD regions, as shown in Fig. S8.

Furthermore, O_3-$PM_{2.5}$PD often exhibited intense atmospheric oxidization (Qin et al., 2021; Dai et al., 2023), and the spatial distribution of the OH concentrations (an important atmospheric oxidant) under the different emission reduction scenarios is shown in Fig. S9. Notably, the reduction in NO_x (VOC) emissions led to an increase (decrease) in the OH concentration in the urban areas, while the effect was the opposite in the non-urban areas. This difference in the OH response to NO_x and VOC emissions between the urban and non-urban areas was caused by their distinct VOC/NO_x sensitivities. In urban areas, where the VOC/NO_x ratio is usually low, OH primarily reacts with NO_x ($NO_2 + OH + M \rightarrow HNO_3 + M$). Thus, reducing NO_x leads to an increase in OH. Conversely, in non-urban areas, which typically exhibit higher VOC/NO_x ratios, OH mainly reacts with VOCs ($RH + OH \rightarrow R^{\bullet} + H_2O$, $RCHO + OH \rightarrow RCO + H_2O$), resulting in an increase in OH with a concurrent decrease in VOCs. Overall, in the BTH and YRD urban areas, reducing VOC emissions not only decreased the occurrence of O_3-$PM_{2.5}$PD but also decreased the atmospheric oxidizing capacity. Notably, in the non-urban areas, particularly in the YRD region, reducing NO_x emissions yielded a similar synergistic benefit.

Since the varied responses of O_3-$PM_{2.5}$PD to reducing the emissions of different precursors could be primarily attributed to the distinct sensitivities of O_3, the differences in the hourly O_3 concentrations during O_3-$PM_{2.5}$PD between the eight emission reduction experiments and the CTRL simulation experiment are shown in Fig. 11. The hourly O_3 concentrations were significantly influenced by the reductions in NO_x and VOC emissions. VOC emission reduction consistently lowered O_3 levels throughout the day, especially the high daytime O_3 concentrations in the urban areas. However, the decrease in night-time O_3 concentrations was greater in the non-urban areas than in the urban areas, largely due to the more notable NO_x titration effect in the urban areas. In contrast, NO_x emission reduction decreased O_3 concentrations only during the day, while O_3 levels increased at night. Enhancing NO_x emission reduction (e.g., by 50 %) extended and amplified the reduction in daytime O_3 concentrations. However, the mitigating effect of NO_x emission reduction on the high daytime O_3 concentrations still remained less significant than that of VOC emission reduction, particularly in the urban areas of the BTH region, where a VOC reduction effectiveness of only approximately 29 %–60 % could be achieved.

Thus far, we have examined the individual impacts of reducing the emissions of different precursors on O_3-$PM_{2.5}$PD and found that reductions in NO_x and VOC emissions play important roles. Therefore, the effect of reducing NO_x and VOC emissions on O_3-$PM_{2.5}$PD simultaneously was further examined, and the results are shown in Fig. 12. The synergistic reduction in NO_x and VOC emissions exerted a greater impact on the decrease in O_3-$PM_{2.5}$PD than the reduction in NO_x or VOC emissions only, except in the BTH urban areas under the scenario with a 25 % emission reduction, which indicated a higher sensitivity to VOC reduction. However, a 50 % reduction in both NO_x and VOC emissions could significantly decrease O_3-$PM_{2.5}$PD in all urban and non-urban areas in the BTH and YRD regions, resulting in decreases of 62.2 % and 72.4 % in the BTH urban and non-urban areas, respectively, and 58.8 % and 72.6 % in the YRD urban and non-urban areas, respectively. Thus, the impact of the synergistic reduction in NO_x and VOC emissions on O_3-$PM_{2.5}$PD was greater than that of reducing NO_x or VOC emissions only, especially in the non-urban areas. These results highlight the significance of the integrated management of NO_x and VOC emissions in both urban and non-urban areas.

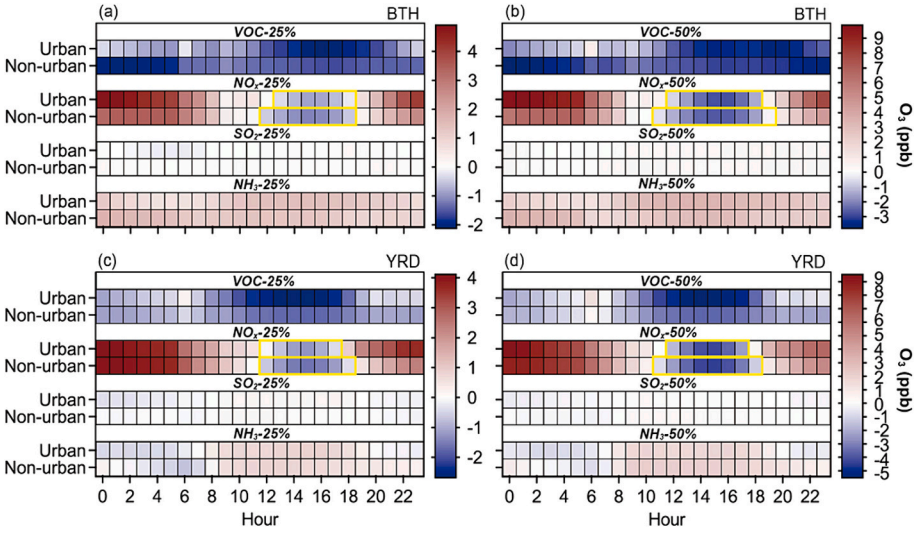

Fig. 11. Difference in the hourly O_3 concentration (ppb) on O_3-$PM_{2.5}$PD between the experiments with reductions of 25 % and 50 % in VOC, NO_x, SO_2, and NH_3 emissions and the CTRL simulation experiment from April–October 2020 averaged over the urban and non-urban areas of the (a-b) BTH and (c-d) YRD regions. The yellow boxes highlight intervals of a decrease in O_3 concentrations by reducing NO_x emissions.

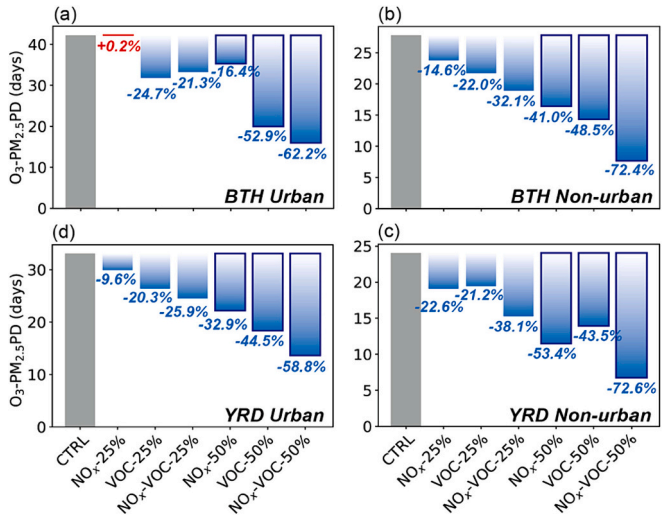

Fig. 12. Frequency of O_3-$PM_{2.5}$PD (days) in the CTRL simulation experiment (grey bars) and changes in O_3-$PM_{2.5}$PD in the eight sensitivity experiments compared to those in the CTRL simulation experiment (shaded blue bars) from April–October 2020 in the urban and non-urban areas of the BTH and YRD regions. The bold italics indicate the percent changes (%) relative to the CTRL simulation experiment.

4. Conclusions

In this study, we conducted multiple sensitivity experiments using the nested-grid version of the GEOS-Chem model to assess the impacts of meteorological factors and anthropogenic emissions on the frequency and intensity of O_3-$PM_{2.5}$PD in the urban and non-urban areas of the BTH and YRD regions from April–October 2013 to 2020. The model generally captured the daily variations in the observed MDA8 O_3 and $PM_{2.5}$ concentrations and reproduced the observed number of O_3-$PM_{2.5}$PD relatively well, with 369 (377) days of observed (simulated) O_3-$PM_{2.5}$PD in the BTH region and 223 (297) days in the YRD region, respectively, summed over April–October 2013–2020. The simulated numbers of O_3-$PM_{2.5}$PD in the urban (non-urban) areas of the BTH and YRD regions were 424.8 (330.1) and 309.3 (286.9) days, respectively, suggesting that pollution in non-urban areas should also be analysed.

From 2013 to 2020, the simulated trends in O_3-$PM_{2.5}$PD in the urban (non-urban) areas of the BTH region were −0.14 (−0.15), −0.99 (−1.23), and +0.30 (−0.19) days yr^{-1} owing to changes in both emissions and meteorological factors, emissions only, and meteorology only, respectively. The corresponding trends in the urban (non-urban) areas of the YRD region were +1.18 (+0.81), −1.47 (−1.92), and +2.11 (+1.50) days yr^{-1}, respectively. These findings suggest that meteorological changes exerted a slight impact on the trend in O_3-$PM_{2.5}$PD in the BTH region and a significant impact on the increasing trend in O_3-$PM_{2.5}$PD in the YRD region from 2013 to 2020, while strict emission reductions since 2013 have led to decreasing trends in anthropogenic emission-driven O_3-$PM_{2.5}$PD in both the BTH and YRD regions, mostly due to the notable reductions in $PM_{2.5}$ concentrations.

We further analysed the influence of the key meteorological parameters on O_3-$PM_{2.5}$PD and identified the main meteorological drivers by utilizing the MLR model. From 2013 to 2020, in most BTH areas, thermodynamic parameters (increase in T2m and T2m_max) were the main drivers of elevated MDA8 O_3 and O_3-$PM_{2.5}$PD levels, while variations in the humidity (decrease in RH1000) and boundary layer dynamics (increase in PBLH) accounted for the reduction in $PM_{2.5}$ concentrations. However, in most YRD areas, an increase in T2m_max affected MDA8 O_3 and O_3-$PM_{2.5}$PD levels, while zonal winds (U500 and U10) played an important role in affecting $PM_{2.5}$ concentrations, which drove a notable increase in O_3-$PM_{2.5}$PD in the YRD region.

In addition, we examined the impact of reductions the emissions of different pollutant precursors (NH_3, SO_2, NO_x, and VOC) on O_3-$PM_{2.5}$PD in 2020 and found that VOC reductions largely reduced O_3-$PM_{2.5}$PD and the atmospheric oxidizing capacity in the urban areas, while NO_x reductions more notably influenced these variables in the non-urban areas, especially in the YRD region. VOC reductions could significantly lower urban O_3 peaks, while NO_x reductions could more effectively reduce non-urban O_3 peaks. Furthermore, a 50 % reduction in both NO_x and VOC emissions could more notably impact O_3-$PM_{2.5}$PD, resulting in decreases of 62.2 % and 72.4 % in the BTH urban and non-urban areas, respectively, and 58.8 % and 72.6 % in the YRD urban and non-urban areas, respectively.

Overall, the meteorological conditions from 2013 to 2020, such as increasing temperatures, significantly amplified the occurrence of O_3-$PM_{2.5}$PD, especially in the BTH and YRD urban areas. Under these pollution-favouring meteorological conditions, emission reductions were more critical for controlling O_3-$PM_{2.5}$PD. Although meteorological conditions and emission sources vary across the different regions, the joint control of NO_x and VOC emissions in both urban and non-urban areas is essential to mitigating O_3-$PM_{2.5}$PD, which have important implications for air quality management. Results from this study may have some limitations and uncertainties. Firstly, model results are dependent on anthropogenic emissions inventories that underlie all the simulations. Secondly, the simulated effectiveness of emission reductions is influenced by the capability of the GEOS-Chem model in simulating chemical species. Previous studies have shown that the model tends to overestimate ammonium levels (Dang and Liao, 2019; Gong and Liao, 2019; Dai et al., 2023). Future studies can use multiple models to provide more comprehensive results.

CRediT authorship contribution statement

Huibin Dai: Writing – original draft, Visualization, Investigation, Formal analysis, Conceptualization. **Hong Liao:** Writing – review & editing, Supervision, Funding acquisition, Conceptualization. **Ye Wang:** Writing – review & editing. **Jing Qian:** Writing – review & editing.

Declaration of competing interest

The authors declare that they have no known competing financial interests or personal relationships that could have appeared to influence the work reported in this paper.

Data availability

All of the measurements, reanalysis data, and GEOS-Chem model code are publicly available from the websites given below. Hourly surface O_3 and $PM_{2.5}$ observations are available at https://quotsoft.net/air/ (last access: 27 November 2023). The dataset of built-up areas of Chinese cities can be obtained from http://www.doi.org/10.11922/sciencedb.j00001.0033 (last access: 27 November 2023). The MERRA-2 reanalysis meteorological dataset is accessible through https://gmao.gsfc.nasa.gov/reanalysis/MERRA-2/ (last access: 27 November 2023). The GEOS-Chem model code can be downloaded through http://acmg.seas.harvard.edu/geos/ (last access: 27 November 2023).

Acknowledgments

This work was supported by the National Natural Science Foundation of China (Grant 42293320). We appreciate the efforts from the GEOS-Chem working groups for developing and managing the model.

Appendix A. Supplementary data

Supplementary data to this article can be found online at https://doi.org/10.1016/j.scitotenv.2024.171687.

References

Alexander, B., Park, R.J., Jacob, D.J., Li, Q.B., Yan-tosca, R.M., Savarino, J., Lee, C.C.W., Thiemens, M.H., 2005. Sulfate formation in sea-salt aerosols: constraints from oxygen isotopes. J. Geophys. Res.-Atmos. 110, D10307 https://doi.org/10.1029/2004jd005659.

Altland, H.W., 1999. Regression analysis: statistical modeling of a response variable. Technometrics 41 (4), 367–368. https://doi.org/10.1080/00401706.1999.10485936.

Bey, I., Jacob, D.J., Yantosca, R.M., Logan, J.A., Field, B.D., Fiore, A.M., Li, Q., Liu, H.Y., Mickley, L.J., Schultz, M.G., 2001. Global modeling of tropospheric chemistry with assimilated meteorology: model description and evaluation. J. Geophys. Res. 106, 23073–23095. https://doi.org/10.1029/2001jd000807.

Che, H., Gui, K., Xia, X., Wang, Y., Holben, B.N., Goloub, P., Cuevas-Agulló, E., Wang, H., Zheng, Y., Zhao, H., Zhang, X., 2019. Large contribution of meteorological factors to inter-decadal changes in regional aerosol optical depth. Atmos. Chem. Phys. 19, 10497–10523. https://doi.org/10.5194/acp-19-10497-2019.

Chen, L., Zhu, J., Liao, H., Yang, Y., Yue, X., 2020. Meteorological influences on $PM_{2.5}$ and O_3 trends and associated health burden since China's clean air actions. Sci. Total Environ. 744, 140837 https://doi.org/10.1016/j.scitotenv.2020.140837.

Dai, H., Zhu, J., Liao, H., Li, J., Liang, M., Yang, Y., Yue, X., 2021. Co-occurrence of ozone and $PM_{2.5}$ pollution in the Yangtze River Delta over 2013-2019: spatiotemporal distribution and meteorological conditions. Atmos. Res. 249, 105363 https://doi.org/10.1016/j.atmosres.2020.105363.

Dai, H., Liao, H., Li, K., Yue, X., Yang, Y., Zhu, J., Jin, J., Li, B., Jiang, X., 2023. Composited analyses of the chemical and physical characteristics of co-polluted days by ozone and $PM_{2.5}$ over 2013-2020 in the Beijing-Tianjin-Hebei region. Atmos. Chem. Phys. 23, 23–39. https://doi.org/10.5194/acp-23-23-2023.

Dang, R., Liao, H., 2019. Severe winter haze days in the Beijing-Tianjin-Hebei region from 1985 to 2017 and the roles of anthropogenic emissions and meteorology. Atmos. Chem. Phys. 19, 10801–10816. https://doi.org/10.5194/acp-19-10801-2019.

Dang, R., Liao, H., Fu, Y., 2021. Quantifying the anthropogenic and meteorological influences on summertime surface ozone in China over 2012-2017. Sci. Total Environ. 754, 142394 https://doi.org/10.1016/j.scitotenv.2020.142394.

Ding, D., Xing, J., Wang, S., Dong, Z., Zhang, F., Liu, S., Hao, J., 2022. Optimization of a NOx and VOC cooperative control strategy based on clean air benefits. Environ. Sci. Technol. 56, 739–749. https://doi.org/10.1021/acs.est.1c04201.

Duan, F., He, K., Ma, Y., Yang, F., Yu, X., Cadle, S.H., Chan, T., Mulawa, P.A., 2006. Concentration and chemical characteristics of PM2.5 in Beijing, China: 2001–2002. Sci. Total Environ. 355, 264–275. https://doi.org/10.1016/j.scitotenv.2005.03.001.

Fairlie, T.D., Jacob, D.J., Park, R.J., 2007. The impact of transpacific transport of mineral dust in the United States. Atmos. Environ. 41, 1251–1266. https://doi.org/10.1016/j.atmosenv.2006.09.048.

Gelaro, R., McCarty, W., Suárez, M.J., Todling, R., Molod, A., Takacs, L., Randles, C.A., Darmenov, A., Bosilovich, M.G., Reichle, R., et al., 2017. The Modern-Era Retrospective Analysis for Research and Applications, version 2 (MERRA-2). J. Clim. 30 (14), 5419–5454. https://doi.org/10.1175/jcli-d-16-0758.1.

Gong, C., Liao, H., 2019. A typical weather pattern for ozone pollution events in North China. Atmos. Chem. Phys. 19, 13725–13740. https://doi.org/10.5194/acp-19-13725-2019.

Gong, C., Liao, H., Yue, X., Ma, Y., Lei, Y., 2021. Impacts of ozone-vegetation interactions on ozone pollution episodes in North China and the Yangtze River Delta. Geophys. Res. Lett. 48, e2021GL093814 https://doi.org/10.1029/2021GL093814.

Guenther, A.B., Jiang, X., Heald, C.L., Sakulyanontvittaya, T., Duhl, T., Emmons, L.K., Wang, X., 2012. The Model of Emissions of Gases and Aerosols from Nature version 2.1 (MEGAN2.1): an extended and updated framework for modeling biogenic emissions. Geosci. Model Dev. 5, 1471–1492. https://doi.org/10.5194/gmd-5-1471-2012.

Hoesly, R.M., Smith, S.J., Feng, L., Klimont, Z., Janssens-Maenhout, G., Pitkanen, T., Seibert, J.J., Vu, L., Andres, R.J., Bolt, R.M., et al., 2018. Historical (1750-2014) anthropogenic emissions of reactive gases and aerosols from the Community Emissions Data System (CEDS). Geosci. Model Dev. 11, 369–408. https://doi.org/10.5194/gmd-11-369-2018.

Jiang, Y., Wang, S., Xing, J., et al., 2022. Ambient fine particulate matter and ozone pollution in China: synergy in anthropogenic emissions and atmospheric processes. Environ. Res. Lett. 17 (12), 123001 https://doi.org/10.1088/1748-9326/aca16a.

Li, K., Jacob, D.J., Liao, H., Shen, L., Zhang, Q., Bates, K.H., 2019. Anthropogenic drivers of 2013-2017 trends in summer surface ozone in China. Proc. Natl. Acad. Sci. U.S.A. 116, 422–427. https://doi.org/10.1073/pnas.1812168116.

Li, K., Jacob, D.J., Shen, L., Lu, X., De Smedt, I., Liao, H., 2020. Increases in surface ozone pollution in China from 2013 to 2019: anthropogenic and meteorological influences. Atmos. Chem. Phys. 20, 11423–11433. https://doi.org/10.5194/acp-20- 11423-2020.

Li, M., Zhang, Q., Kurokawa, J., Woo, J.-H., He, K., Lu, Z., Ohara, T., Song, Y., Streets, D. G., Carmichael, G.R., et al., 2017. MIX: a mosaic Asian anthropogenic emission inventory under the international collaboration framework of the MICS-Asia and HTAP. Atmos. Chem. Phys. 17 (2), 935–963. https://doi.org/10.5194/acp-17-935-2017.

Luo, Y., Zhao, T., Yang, Y., Zong, L., Raghavendra Kumar, K., Wang, H., Meng, K., Zhang, L., Lu, S., Xin, Y., 2022. Seasonal changes in the recent decline of combined high $PM_{2.5}$ and O_3 pollution and associated chemical and meteorological drivers in the Beijing-Tianjin-Hebei region, China. Sci. Total Environ. 838, 156312. https://doi.org/10.1016/j.scitotenv.2022.156312.

Ma, X., Yin, Z., Cao, B., Wang, H., 2023. Meteorological influences on co-occurrence of O_3 and $PM_{2.5}$ pollution and implication for emission reductions in Beijing-Tianjin-Hebei. Sci. China Earth Sci. 66, 1258–1267. https://doi.org/10.1007/s11430-022-1070-y.

Mao, J.Q., Crounse, J.D., Jacob, D.J., Cohen, R.C., Crounse, J.D., Wennberg, P.O., Keller, C.U., Hudman, R.C., Barkley, M.P., Horowitz, L.W., 2013. Ozone and organic nitrates over the eastern United States: sensitivity to isoprene chemistry. J. Geophys. Res.-Atmos. 118, 11256–11268. https://doi.org/10.1002/jgrd.50817.

Ministry of Ecology and Environment of the People's Republic of China, 2021. China Statistical Yearbook. http://www.mee.gov.cn/hjzl/sthjzk/zghjzkgb/. (Accessed 13 March 2024).

Ni, R., Lin, J., Yan, Y., Lin, W., 2018. Foreign and domestic contributions to springtime ozone over China. Atmos. Chem. Phys. 18 (11447–11469) https://doi.org/10.5194/acp-18-11447-2018.

Ou, S., Wei, W., Cai, B., Yao, S., Wang, K., Cheng, S., 2022. Exploring the causes for co-pollution of O_3 and $PM_{2.5}$ in summer over North China. Environ. Monit. Assess. 194, 289. https://doi.org/10.1007/s10661-022-09951-4.

Park, R.J., 2003. Sources of carbonaceous aerosols over the United States and implications for natural visibility. J. Geophys. Res. 108 (D12) https://doi.org/10.1029/2002jd003190.

Park, R.J., 2004. Natural and transboundary pollution influences on sulfate-nitrate-ammonium aerosols in the United States: implications for policy. J. Geophys. Res. 109, D15. https://doi.org/10.1029/2003jd004473.

Pye, H., Liao, H., Wu, S., Mickley, L.J., Jacob, D.J., Henze, D.K., Seinfeld, J.H., 2009. Effect of changes in climate and emissions on future sulfate-nitrate-ammonium aerosol levels in the United States. J. Geophys. Res. 114 (d1) https://doi.org/10.1029/2008jd010701.

Qian, J., Liao, H., Yang, Y., Li, K., Chen, L., Zhu, J., 2022. Meteorological influences on daily variation and trend of summertime surface ozone over years of 2015-2020: quantification for cities in the Yangtze River Delta. Sci. Total Environ. 834 (155107), 2022. https://doi.org/10.1016/j.scitotenv.2022.155107.

Qin, Y., Li, J.Y., Gong, K.J., Wu, Z., Chen, M.D., Qin, M.M., Huang, L., Hu, J.L., 2021. Double high pollution events in the Yangtze River Delta from 2015 to 2019: characteristics, trends, and meteorological situations. Sci. Total Environ. 792, 148349 https://doi.org/10.1016/j.scitotenv.2021.148349.

Shao, M., Yang, J., Wang, J., Chen, P., Liu, B., Dai, Q., 2022. Co-occurrence of surface O_3, $PM_{2.5}$ pollution, and tropical cyclones in China. J. Geophys. Res. Atmos. 127 (14) https://doi.org/10.1029/2021JD036310.

Shen, L., Mickley, L.J., Tai, A.P.K., 2015. Influence of synoptic patterns on surface ozone variability over the eastern United States from 1980 to 2012. Atmos. Chem. Phys. 15 (19), 10925–10938. https://doi.org/10.5194/acp-15-10925-2015.

State Council of the People's Republic of China, 2013. Action Plan on Air Pollution Prevention and Control (in Chinese). http://www.gov.cn/zwgk/2013-09/12/content_2486773.htm. (Accessed 13 March 2024).

State Council of the People's Republic of China, 2018. Action Plan on Air Pollution Prevention and Control (in Chinese). http://www.mee.gov.cn/ywdt/hjywnews/201807/t20180704_446065.shtml. (Accessed 13 March 2024).

Sun, J., Sun, Z., Guo, H., Wang, J., Jiang, H., Gao, H., 2022. A dataset of built-up areas of Chinese cities in 2020. China Sci. Data 7 (1). https://doi.org/10.11922/11-6035.csd.2021.0087.zh.

Wang, L., Chang, J., Zheng, X., Liu, J., Yu, M., Liu, L., Yang, Y., Zhang, H., 2018. Survey of ecological environmental conditions and influential factors for public parks in Shanghai. Chemosphere 190, 9–16. https://doi.org/10.1016/j.chemosphere.2017.09.061.

Wang, P., Guo, H., Hu, J., Kota, S.H., Ying, Q., Zhang, H.L., 2019. Responses of $PM_{2.5}$ and O_3 concentrations to changes of meteorology and emissions in China. Sci. Total Environ. 662, 297–306. https://doi.org/10.1016/j.scitotenv.2019.01.227.

Xuan, J., Liu, G., Du, K., 2000. Dust emission inventory in northern China. Atmos. Environ. 34, 4565–4570. https://doi.org/10.1016/S1352-2310(00)00203-X.

Yang, Y., Liao, H., Lou, S.J., 2016. Increase in winter haze over eastern China in recent decades: roles of variations in meteorological parameters and anthropogenic emissions. J. Geophys. Res. Atmos. 121 (21), 13050–13065. https://doi.org/10.1002/2016JD025136.

Ye, B., Ji, X., Yang, H., Yao, X., Chan, C.K., Cadle, S.H., Chan, T., Mulawa, P.A., 2003. Concentration and chemical composition of $PM_{2.5}$ in Shanghai for a 1-year period. Atmos. Environ. 37, 499–510. https://doi.org/10.1016/S1352-2310(02)00918-4.

Yin, P., Chen, R., Wang, L., Meng, X., Liu, C., Niu, Y., Lin, Z., Liu, Y., Liu, J., Qi, J., You, J., Zhou, M., 2017. Ambient ozone pollution and daily mortality: a nationwide study in 272 Chinese cities. Environ. Health Perspect. 125 (11), 117006 https://doi.org/10.1289/EHP1849.

Yue, X., Unger, N., Harper, K., Xia, X., Liao, H., Zhu, T., Xiao, J., Feng, Z., Li, J., 2017. Ozone and haze pollution weakens net primary productivity in China. Atmos. Chem. Phys. 17, 6073–6089. https://doi.org/10.5194/acp-17-6073-2017.

Zhang, Q., Zheng, Y., Tong, D., et al., 2019b. Drivers of improved $PM_{2.5}$ air quality in China from 2013 to 2017. Proc. Natl. Acad. Sci. U.S.A. 116, 24463–24469. https://doi.org/10.1073/pnas.1907956116.

Zhang, Y., Wang, Y., 2016. Climate-driven ground-level ozone extreme in the fall over the Southeast United States. Proc. Natl. Acad. Sci. U.S.A. 113, 10025–10030. https://doi.org/10.1073/pnas.1602563113.

Zhang, Y., Guo, Y., Li, G., Zhou, J., Jin, X., Wang, W., Pan, X., 2019a. The spatial-temporal characteristics and health impacts of ambient fine particulate matter in China. J. Clean. Prod. 213, 585–594. https://doi.org/10.1016/j.jclepro.2015.05.006.

Zhao, X.J., Zhao, P.S., Xu, J., Meng, W., Pu, W.W., Dong, F., He, D., Shi, Q.F., 2013. Analysis of a winter regional haze event and its formation mechanism in the North

China Plain. Atmos. Chem. Phys. 13, 5685–5696. https://doi.org/10.5194/acp-13-5685-2013.

Zheng, B., Tong, D., Li, M., Liu, F., Hong, C., Geng, G., Li, H., Li, X., Peng, L., Qi, J., Yan, L., Zhang, Y., Zhao, H., Zheng, Y., He, K., Zhang, Q., 2018. Trends in China's anthropogenic emissions since 2010 as the consequence of clean air actions. Atmos. Chem. Phys. 18, 14095–14111. https://doi.org/10.5194/acp-18-14095-2018.

Zheng, B., Zhang, Q., Geng, G., Chen, C., Shi, Q., Cui, M., Lei, Y., He, K., 2021. Changes in China's anthropogenic emissions and air quality during the COVID-19 pandemic in 2020. Earth Syst. Sci. Data 13, 2895–2907. https://doi.org/10.5194/essd-13-2895-2021.